A SiC-Based Converter as a Utility Interface for a Battery System

Hui Zhang[1], Leon M. Tolbert[1,2], Burak Ozpineci[2], Madhu S. Chinthavali[2]

hzhang18@utk.edu, tolbert@utk.edu, ozpinecib@ornl.gov, chinthavalim@ornl.gov

[1]Electrical and Computer Engineering
The University of Tennessee
Knoxville, TN 37996-2100

[2] Power Electronics & Electric Machinery Research Center
Oak Ridge National Laboratory
Knoxville, TN 37932

***Abstract* — The purpose of this work is to provide validated models to estimate the performance of a SiC-based converter as a utility interface in battery systems. System design and modeling are described in detail. Simulations are done for both a SiC JFET converter and its Si counterpart based on the quality of tested devices. The simulation results indicate that in both charging and discharging modes, the SiC converter has a better performance compared to the Si one. (1) With the same heatsink size and ambient temperature, great advantages in efficiency and junction temperatures were found in the SiC-based converter. (2) With the same thermal limit, large savings in system weight and volume combined with a high efficiency were found in the SiC-based converter.**

***Keywords* — Silicon carbide (SiC), JFET, Schottky diode, inverter, modeling, battery.**

I. Introduction

Silicon carbide (SiC), as an alternative choice of material for power electronics, has been widely known. It has advantages in electrical breakdown field, thermal conductivity, electron saturated drift velocity, and irradiation tolerance. These make the SiC devices able to work at higher voltage, temperature, and frequency, and produce less power losses at the same time. As a result, a system composed of SiC devices is more efficient and reliable. Therefore, SiC power electronics devices are expected to substitute for Si counterparts in high-power, high-temperature, and high-frequency applications [1-4]. At present, most SiC applications focus on military, aerospace, and geothermal, where cost is not a critical factor. Utility and automobiles are two other potential applications, which are drawing more attention. As the cost of SiC devices decreases, there will be more application areas for SiC devices.

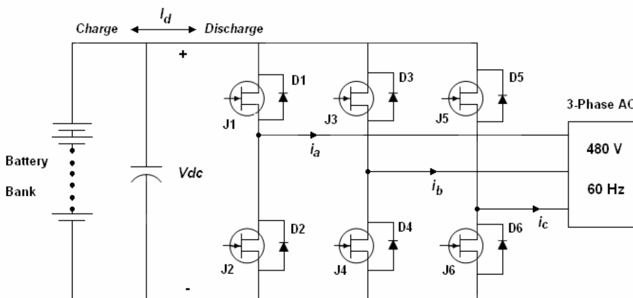

Fig. 1. Inverter interface system structure.

A qualitative description of SiC devices is not enough to guide device designers and customers. Device, circuit, and system models and specific quantitative results for different applications are required. In this work, simulations of a SiC-based converter working as an interface between a battery bank and a utility were performed. Quantitative advantages of this system compared to its Si counterpart were obtained based on the quality of tested devices.

II. Utility Interface System Design

The utility interface system is composed of a battery bank and a converter. The battery bank is to be charged and discharged from the utility via the three-phase, full-bridge converter (refer to Fig. 1). The converter works as a rectifier during the charging of the battery, and an inverter for discharging.

A. DC Link Voltage

The converter is controlled by Sinusoidal Pulse Width Modulation strategy (SPWM). The relationship between line voltage, V_{ll}, and dc link voltage, V_{dc}, can be expressed as (1), where M is modulation index [5]. If $0 \le M \le 1$, the minimum dc link voltage is for $M = 1$. For $V_{ll} = 480$ V, $V_{dc\,(min)} = 783.8$ V.

$$V_{ll} = M \cdot \frac{\sqrt{3}V_{dc}}{2\sqrt{2}} \tag{1}$$

B. Battery Bank

The battery bank must be designed to meet the minimum requirement of the dc link voltage. A Hawker Genesis brand, 13Ah rated lead acid battery (with a nominal voltage of 12V) is considered here. Its property curves are shown in Fig. 2 [6]. During discharging, the output voltage of the battery slowly decreases due to the decrease of open-circuit voltage of the battery. Thus, at the end of discharge, the open-circuit voltage of the battery is the minimum, and this determines the number of batteries needed in series. As shown as Fig. 2(c), after the battery is discharged to about 40% state of charge (SOC), there will be a sharp increase in battery discharge resistance. Consequently, running the battery with a SOC lower than 40% would require a large number of batteries in series. Specifically, the number of batteries in series can be 43% more when the batteries are discharged to 20% SOC instead of 40%

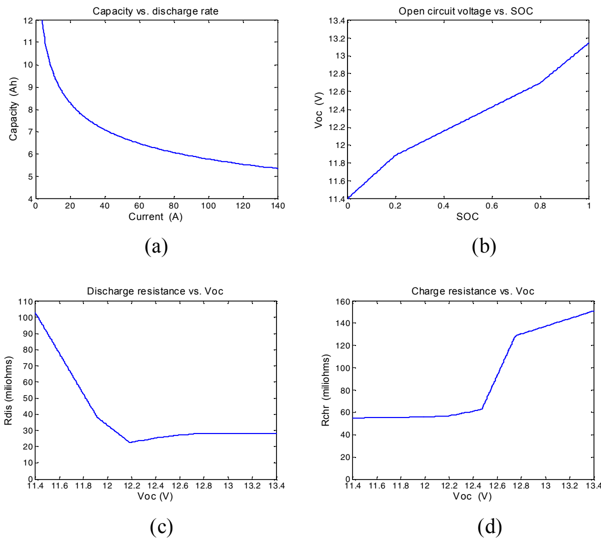

Fig. 2. Characteristics of Hawker Genesis battery (13Ah).

SOC. Therefore, the optimum number of batteries in series is 84 corresponding to the end of discharge at 40% SOC in this case. If the battery bank is discharged by a constant current of 120 A, it can last 2.33 hours from full charge to 40% SOC.

C. Converter

The converter has a standard 3-phase full-bridge topology with six switches and six anti-parallel diodes. To meet the requirements of this system, the ratings of these devices must be larger than the maximum of the current and the voltage that they are supposed to handle. The maximum voltage occurs when the batteries are fully charged, and this value is larger than the nominal voltage of batteries. The maximum current occurs at the beginning of the discharge of batteries. Based on the above discussion and also considering the availability of devices, the selected devices are shown in Table I.

TABLE I. DEVICES USED IN THE CONVERTERS

Item	Voltage rating	Current rating	Part number
SiC JFETs	1200	14A ×21	SiCED
SiC Schottky diodes	1200	10A×30	Cree, CSD10120
Si IGBT Module	1200	300A	Powerex, CM300DY-24NF

III. MODELING

Fig. 3 shows the modeling methodology of this system. The battery model and converter model are the two basic components.

A. Converter Model

The converter models have three parts, namely single device models, converter power loss models, and thermal models. Single device models are the basis of the converter models, which describe device characteristics in both conduction and switching periods under different temperatures. The converter power loss models use an averaging technique to estimate the system power loss under a specific control strategy. Their inputs are device characteristics given by single device models and the system operation variables (converter dc side voltage, ac side current, modulation index, and power factor) calculated by the battery model. Their outputs are the power losses of switches and diodes. These power losses are input into the thermal models to get real-time junction temperatures of devices. At the same time, the temperatures are fed back to the single device models in order to update device characteristics. A brief summary of specific mathematical models is presented in Appendix II. More details can be found in papers [7-11].

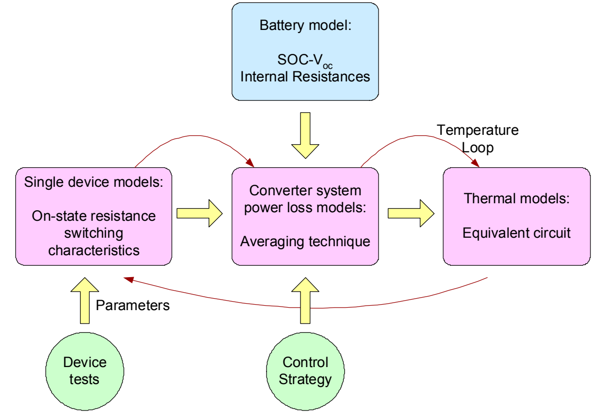

Fig. 3. Modeling methodology for battery-converter system.

B. Battery Model

Developing a battery model is beyond this work. It is reasonable to use a basic equivalent circuit shown in Fig. 4 to describe the performance of batteries. This information is only needed to generate approximate voltage and current levels expected from a typical battery. The parameters of Hawker Genesis batteries used in this system are from [6].

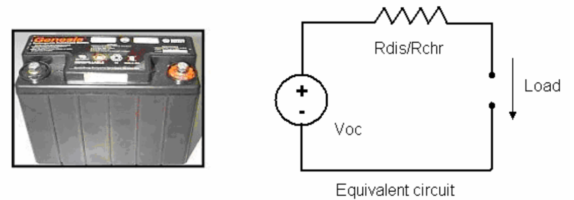

Fig. 4. Hawker Genesis battery (13Ah, 12V) and its equivalent circuit.

IV. SIMULATIONS AND DISCUSSIONS

In this work, the utility has a line voltage of 480 Vrms, a frequency of 60 Hz, and the converter was controlled to produce current at unity power factor. The battery bank is composed of 84 13Ah Hawker Genesis batteries in series. The battery bank is discharged at a constant current of 120 A from full charge to 40% SOC, and the power is delivered to the utility through the converter. Vice versa, it is charged at a

constant voltage of 1109 V from 40% SOC to full charge, and the power is provided by the utility through the converter. In both discharge and charge processes, the converter works as an interface. They are expected to consume as little power as possible. The power losses and efficiencies of the SiC and Si converters based on the devices in Table I were computed for different conditions using the technique presented in Part III. Some parameters obtained from device tests used in the simulations are listed in Table II.

TABLE II. DEVICE CHARACTERISTICS (AT ROOM TEMPERATURE)

Characteristics	Si	SiC
IGBT/JFET on-state resistance	6.6 mΩ	7.4 mΩ (0.156Ω/21)
IGBT/JFET voltage drop when I=0	0.83 V	0.0
IGBT/JFET transconductance	61.2 S	14.7 S (0.7 S×21)
Diode on-state resistance	8.6 mΩ	2.1 mΩ (63.8mΩ/30)
Diode reverse recovery charge	13μC	0.84μC (28nC×30)

Using MATLAB Simulink, two sets of simulations have been done for both the SiC-based and Si-based systems for a charge cycle and a discharge cycle, respectively. In the first set of simulations, the ambient temperatures and the heatsink sizes were the same for the Si and SiC systems. In the second set of simulations, the heatsinks were selected to limit the maximum junction temperature to 125°C for both the SiC and Si devices.

Based on the specific system information discussed previously, the battery system model worked out the unknown system parameters required for power losses calculation. As shown as Fig. 5 (a), the peak current flowing through the converters changed slowly during the discharge cycle. While it decreased quickly as the open-circuit voltage of the battery bank increased during the charge cycle, and the average of the charge current is much lower than that of the discharge current (Fig. 5 (b)). Thus, the charge cycle is much longer than the discharge cycle, and the power involved in the charge cycle is much lower than that in the discharge cycle.

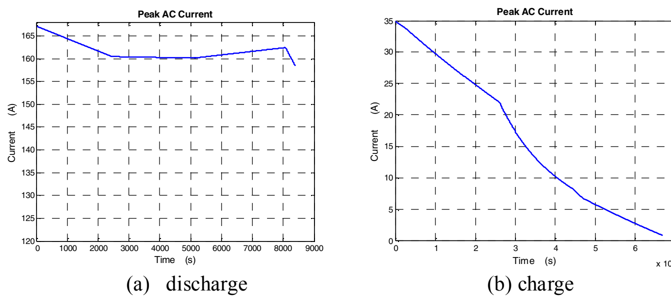

(a) discharge (b) charge

Fig. 5. AC side current under two modes (100% - 40% SOC).

A. With the Same Heatsink Size and Ambient Temperature

With variation of the system variables, power losses, device junction temperatures and parameters change dynamically. The change processes obtained from simulations are shown in Figs. 6-9 (for discharge) and Figs. 10-13 (for charge).

During discharge, the great power savings of the SiC Schottky diode due to lower on-state resistance (Fig. 7 (b)) and better reverse recovery characteristics reduced the temperature rise of the SiC system dramatically (Fig. 6). Temperature has a significant effect on device characteristics, especially on the mobility of electrons and holes that dominates the dependency on temperature of the on-state resistance of devices. Although the on-state resistance of the SiC JFET is larger than that of the Si IGBT at room temperature (see Table II), a lower on-state resistance was found in the SiC JFET as shown in Fig. 7 (a) because of its much lower junction temperature (see Fig. 6 (a)).

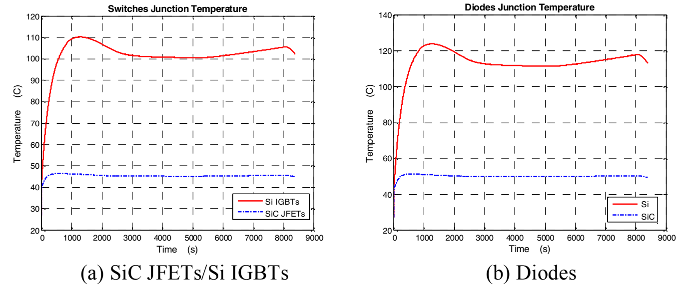

(a) SiC JFETs/Si IGBTs (b) Diodes

Fig. 6. Device junction temperatures during discharge.

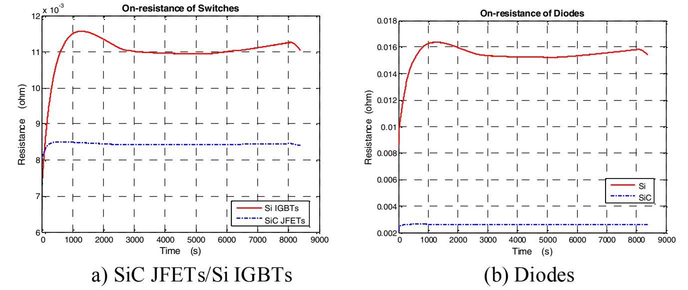

a) SiC JFETs/Si IGBTs (b) Diodes

Fig. 7. Device on-state resistances during discharge.

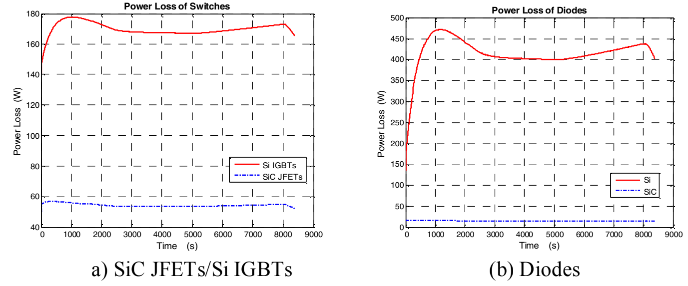

a) SiC JFETs/Si IGBTs (b) Diodes

Fig. 8. Device power losses during discharge (single device).

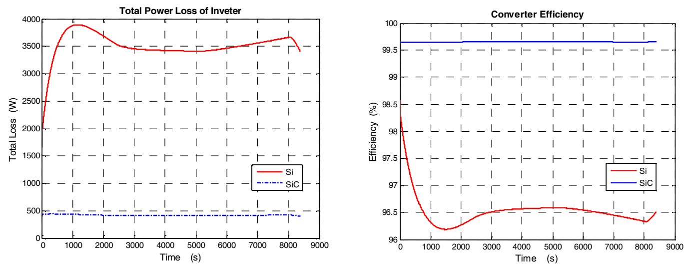

Fig. 9. System power losses and efficiency during discharge.

This further reduced system power losses and improved efficiency of the SiC converter (see Fig. 8 and Fig. 9). Consequently, the junction temperature rise of the SiC devices is less than that of the Si devices (refer to Appendix II). As shown in Fig. 3, the junction temperatures continued to affect the device characteristics, and repeat the above dynamic process until a steady state is reached.

During charge, a similar process exists. Again, the performance of the SiC Schottky diode is much better than that of the Si diode in both conduction and switching states (Figs. 10-12 (b)). For the SiC JFET, its on-state resistance is larger than that of the Si IGBT in most of the period as shown in Fig. 11 (a). It seems that the conduction loss of the SiC JFET should be larger. However, this is not the only contribution to the conduction loss of a switch. The loss due to the voltage drop across Schottky barrier or *pn*-junction is also an important part, and it dominates when current is small (refer to the equations in Appendix II). As the device characteristics provided in Table II, the voltage drop across the Si IGBT at zero current is much higher than that of the SiC JFET. So the conduction loss of the Si IGBT due to this voltage drop is relatively large. Since the current during charge is small, this part of conduction loss dominates the overall conduction loss. That is to say, the overall conduction loss of the SiC JFET is smaller than that of the Si IGBT. As for switching losses, the SiC JFET can also compete with the Si IGBT because of no tail current during turn off. Thus, the total of power losses of the SiC JFET is smaller than that of the Si IGBT as shown in Fig. 12(a). Combining the better performances of the SiC JFET and the SiC Schottky diode, the SiC converter is better than the Si one under charge mode (see Fig. 13).

No matter discharge mode or charge mode, the SiC converter shows better performance than the Si one in efficiency and juncture temperature. More clearly, the specific improvements are summarized in Table III.

TABLE III. COMPARISON OF SIC AND SI CONVERTER

Operation Mode	Average Junction temperature reduction (°C)	Average efficiency improvement (%)	Average power loss reduction (kW)	Energy savings in one cycle (kWh)
Condition A: With the same heatsink size and ambient temperature				
Discharge	56/63	3.3	3.09	7.20
Charge	7/11	5.5	0.45	8.37
Condition B: With the same maximum junction temperature (125°C)				
Discharge	4/3	3.1	2.93	6.83
Charge	1/5	5.4	0.45	8.30

Note: The two numbers in column "Junction temperature reduced" are for JFET(IGBT) and diode, respectively.

B. *With Different Sizes of Heatsinks*

In high power applications, the size of a heatsink could account for 1/3 of total system volume. How to reduce the size of heatsink is always an issue. To show the benefit of a SiC converter in this aspect, the simulation is designed to run the SiC and Si devices to the same temperature (125°C) by using different sizes of heatsinks. The results indicate that the size of the heatsink required by the SiC converter is reduced to about 1/25 of that of the Si converter under the same cooling method (forced cooling with fan) or 4/5 when the SiC inverter is naturally cooled, and at the same time the efficiency is improved by 3.1% for discharge, 5.4% for charge.

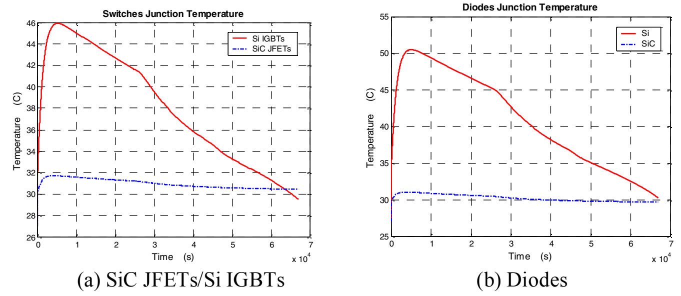

(a) SiC JFETs/Si IGBTs (b) Diodes

Fig. 10. Device junction temperatures during charge.

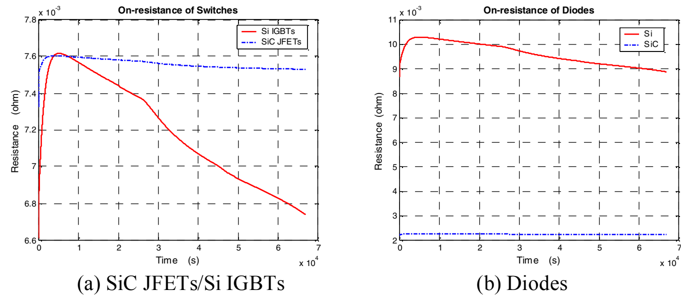

(a) SiC JFETs/Si IGBTs (b) Diodes

Fig. 11. Device on-state resistances during charge.

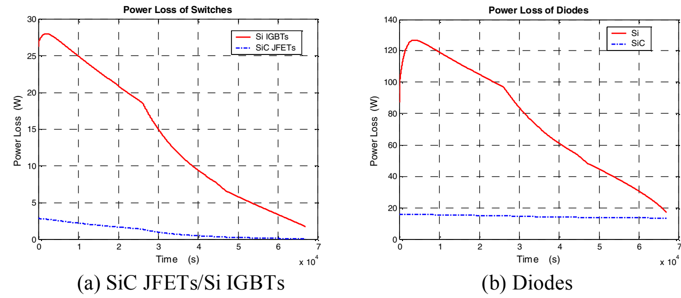

(a) SiC JFETs/Si IGBTs (b) Diodes

Fig. 12. Device power losses during charge (single device).

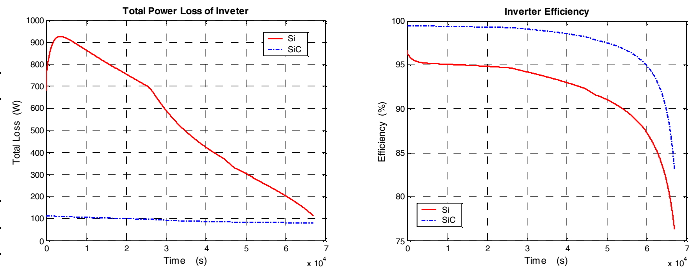

Fig. 13. System power losses and efficiency during charge.

In addition, when the average junction temperatures of SiC devices change from 45°C /50°C (for the SiC JFET/the SiC Schottky diode, respectively) under Condition A (in Table III) to 97°C /116°C under Condition B, the efficiency of the SiC converter during discharge is lowed by only 0.2%. This indicates that the influence of temperature on the SiC devices is

very small. Thus, more benefits can be achieved if SiC devices are used in high-temperature applications.

V. CONCLUSIONS

In both charging and discharging modes, the SiC converter has a better performance over the Si one. With the same external thermal condition (the same heatsink size and ambient temperature), great advantages in efficiency and junction temperatures were found for the SiC-based converter. On the other hand, with the same thermal limit, large savings in system weight and volume combined with a high efficiency were found in the SiC-based converter. Therefore, this SiC-based battery converter system is expected to substitute for its Si counterpart in systems like automobiles where weight and volume are the critical factors, the SiC converter can be designed with a simple and compact cooling system. For solar systems where efficiency and reliability is more important, the SiC converter can have a normal cooling system in order to achieve high efficiency and reliability. Even though SiC devices are expensive, the large savings can make them very cost-effective.

REFERENCES

[1] L. M. Tolbert, B. Ozpineci, S. K. Islam, M. Chinthavali, "Wide bandgap semiconductors for utility applications," *IASTED International Conference on Power and Energy Systems (PES 2003)*, February 24-26, 2003, Palm Springs, California, pp. 317-321.

[2] NEDO, "Development of ultra low loss power devices technology," www.nedo.go.jp/kankobutsu/ pamphlets/shindenryoku/development.pdf.

[3] T. Ericsen, "Future navy application of wide bandgap power semiconductor devices," *Proceedings of the IEEE*, vol. 90, Issue 6, June 2002, pp. 1077-1082.

[4] P. G. Neudeck, L. G. Matus, "An overview of silicon carbide device technology," *Ninth Symposium on Space Nuclear Power Systems*, Albuquerque, New Mexico, Jan. 12-16, 1992.

[5] N. Mohan, T. M. Undeland, W. P. Robbins, *Power Electronics*, 2nd Edition, John Wiley & Sons Inc., 1995.

[6] V. Johnson, M. Keyser, "Testing, analysis, and validation of a Hawker Genesis lead acid battery model in ADVISOR," www.ctts.nrel.gov/ analysis/documents/hawker_validation.html, Mar. 1999.

[7] H. Zhang, M. Chinthavali, B. Ozpineci, L. M. Tolbert, "Power losses and thermal modeling of 4H-SiC VJFET inverter," *IEEE Industry Applications Society Annual Meeting,* October 2-6, 2005, Hong Kong, China, pp. 2630-2634.

[8] F. Blaabjerg, J. K. Pedersen, "Optimized design of a complete three phase PWM-VS Inverter," *IEEE Transactions on Power Electronics*, vol. 12, no. 3, May 1997, pp. 567-577.

[9] C. Wong, "EMTP modling of IGBT dynamic performance for power dissipation estimation," *IEEE Transactions on Industry Applications*, vol. 33, no. 1, Jan./Feb. 1997, pp64-71.

[10] V. Blasko, R. Lukaszewski, R. Sladky, "On line thermal model and thermal management strategy of a three phase voltage source inverter," *IEEE Industry Applications Society Annual Meeting*, October 3-7, 1999, Phoenix, Arizona, pp.1423-1431.

[11] B. Ozpineci, *System Impact of Silicon Carbide Power Electronics on Hybrid Electric Vehicle Applications*, Ph.D dissertation, The University of Tennessee, Aug. 2002.

APPENDIX I. SYMBOLS

V_D	Diode voltage when current is 0	E_c	Breakdown voltage
V_I	IGBT voltage when current is 0	ε	Dielectric constant
R_D	On resistance of diode	V_{dc}	DC bus voltage
R_J	On resistance of JFET	g_m	Transconductance
R_I	On resistance of IGBT	V_{GH}	Highest gate voltage
I	Peak forward current	V_{GL}	Lowest gate voltage
J	Current density	V_{th}	Threshold voltage
M	Modulation index	P_j	Power loss of JFET/IGBT
ϕ	Phase angle of current	P_d	Power loss of diode
f_c	Switching frequency	R_{jc}	Thermal resistance from junction to case
t_{tail}	Duration of tail current of IGBT		
k_t	Tail current factor for IGBT	R_{ch}	Thermal resistance from case to heatsink
I_R	Peak reverse current of diode		
t_{rr}	Reverse recovery time of diode	R_{ha}	Thermal resistance from heatsink to ambient
S	Snappiness factor of diode		
A	Active area of device	C	Thermal capacitance

APPENDIX II. MODELING OF INVERTER

1. IGBT

Conduction loss: $$P_{cond,I} = I^2 \cdot R_I \left(\frac{1}{8} + \frac{1}{3\pi} M\cos\phi\right) + I \cdot V_I \cdot \left(\frac{1}{2\pi} + \frac{M\cos\phi}{8}\right) + \left(\frac{dI_R}{dt}\right)^2 \cdot \frac{f_c t_{rr}^{\ 3}}{3(S+1)^2} \cdot R_I$$

Switching loss: $$P_{sw,J} = \frac{f_c}{2\pi}\left\{\begin{array}{l} \dfrac{H\cdot G_1}{\sqrt{G_1^{\ 2} - I^2}}\left[\pi + 2\tan^{-1}\left(\dfrac{I}{\sqrt{G_1^{\ 2}-I^2}}\right)\right] \\ + \dfrac{H\cdot G_2}{\sqrt{G_2^{\ 2} - I^2}}\left[-\pi + 2\tan^{-1}\left(\dfrac{I}{\sqrt{G_2^{\ 2}-I^2}}\right)\right] \\ + k_t \cdot I \cdot V_{dc} \cdot t_{tail} \end{array}\right\}$$

$$H = \frac{1}{3}\varepsilon E_c V_{dc} A \left(\frac{V_{dc}}{V_B}\right)^{1/2} \quad G_1 = g_m(V_{GH} - V_{th}) \quad G_2 = g_m(V_{th} - V_{GL})$$

2. JFET

Conduction loss: $$P_{cond,J} = I^2 \cdot R_J \left(\frac{1}{8} + \frac{1}{3\pi} M\cos\phi\right) + \left(\frac{dI_R}{dt}\right)^2 \cdot \frac{f_c t_{rr}^{\ 3}}{3(S+1)^2} \cdot R_J$$

Switching loss: $$P_{sw,J} = \frac{Hf_c}{2\pi}\left\{\begin{array}{l} \dfrac{G_1}{\sqrt{G_1^{\ 2} - I^2}}\left[\pi + 2\tan^{-1}\left(\dfrac{I}{\sqrt{G_1^{\ 2}-I^2}}\right)\right] \\ + \dfrac{G_2}{\sqrt{G_2^{\ 2} - I^2}}\left[-\pi + 2\tan^{-1}\left(\dfrac{I}{\sqrt{G_2^{\ 2}-I^2}}\right)\right] \end{array}\right\}$$

3. Diode

Conduction loss: $$P_{cond,D} = I^2 \cdot R_D \left(\frac{1}{8} - \frac{1}{3\pi} M\cos\phi\right) + I \cdot V_D \cdot \left(\frac{1}{2\pi} - \frac{M\cos\phi}{8}\right)$$

Switching loss: $$P_{sw,D} = f_c \cdot \frac{V_{dc}}{2S}\left(\frac{dI_R}{dt}\right)\left(\frac{St_{rr}}{S+1}\right)^2$$

4. Thermal Model